# Distinct Onset Mechanisms of Two Subtypes of CP El Niño and Their Changes in Future Warming

**Mengyan Chen[1]**, **Jin-Yi Yu[2]**, **Xin Wang[1,3]**, and **Sheng Chen[1,3]**

[1]State Key Laboratory of Tropical Oceanography, South China Sea Institute of Oceanology, Chinese Academy of Sciences, Guangzhou, China, [2]Department of Earth System Science, University of California, Irvine, CA, USA, [3]Southern Marine Science and Engineering Guangdong Laboratory (Guangzhou), Guangzhou, China

**Abstract** This study analyzes two subtypes of Central Pacific (CP) El Niño and shows that they possess different sea surface temperature evolution patterns in the Indo-Pacific Oceans, distinct generation mechanisms, and can respond differently to global warming. The CP-I type is triggered in the tropical western Pacific by the weaker-than-normal Australian winter monsoon (AM) through a subsurface thermocline mechanism and is accompanied by significant Indian Ocean warming. The CP-II type onsets in the subtropical North Pacific by the Pacific Meridional Mode (PMM) through a surface coupling mechanism and is accompanied by weak warming anomalies in the Indian Ocean. Two climate models projections indicate that the CP-II type may occur more frequently than the CP-I type in the future due to changes in PMM and AM activities, which should weaken El Niño influences on the Indian Ocean and result in more El Niño events that onset from the North American coast.

**Plain Language Summary** It is well known that El Niño can be divided into conventional eastern Pacific (EP) El Niño and the emerging central Pacific (CP) El Niño. More recently, researchers suggested that the CP El Niño can be separated into two subtypes based on their distinct evolution of SST anomalies and climate impacts. In this study, we show that the two subtypes of CP El Niño possess different generation mechanisms. The CP-I El Niño onsets from the far western tropical Pacific and it is trigged by the Australian monsoon, while the CP-II El Niño originates from the subtropical North Pacific and is triggered by the Pacific Meridional Mode. The weaker-than-normal Australian winter monsoon can induce the positive sea surface height (SSH) anomalies in the far western tropical Pacific via the reduced Indonesian Throughflow transports from the tropical Pacific to the Indian Ocean. The SSH anomalies then excite eastward propagated downwelling Kelvin waves and induce warming anomalies in the central equatorial Pacific. The Pacific Meridional Mode (PMM) generates the CP-II El Niño via a surface atmosphere-ocean interaction. CMIP5 models project that the CP-II type will occur more frequently than the CP-I type in the future due to changes in PMM and Australian winter monsoon activities.

## 1. Introduction

It is now generally recognized that El Niño can be divided into Eastern Pacific (EP) and Central Pacific (CP) types based on the central zonal location of its largest sea surface temperature (SST) anomalies. The CP El Niño has its largest SST anomalies in the tropical central Pacific, which is different from EP El Niño that has its largest SST anomalies off the coast of the South American coast (Capotondi et al., 2015; Yu et al., 2017). The CP El Niño has occurred more frequently during recent decades (Lee & McPhaden, 2010; Yeh, Wang, et al., 2015; Yu et al., 2012) and its distinct properties challenge our conventional views of and approaches to El Niño dynamics, impacts, and predictions (Capotondi et al., 2015; Yu & Fang, 2018; Yu et al., 2017). Recent studies have suggested that CP El Niños can be further divided into CP-I and CP-II types based on their different SST anomaly structures and climate impacts (Chen, Chang, et al., 2021; Chen, Yu, et al., 2019; Tan, Wang, et al., 2016; Tan, Wei, et al., 2020; C. Wang & Wang, 2013; X. Wang & Wang, 2014). Warm SST anomalies during CP-I events develop mostly in the central tropical Pacific but during CP-II events extend into the subtropical northeastern Pacific (C. Wang & Wang, 2013). The two types of events produce distinct impacts on the Indian Ocean Dipole (X. Wang & Wang, 2014), South China Sea SSTs (Tan, Wang, et al., 2016), East Asian Winter Monsoon (J.-W. Kim et al., 2021), and western Pacific subtropical high (WPSH; Chen, Chang, et al., 2021; Chen, Yu, et al., 2019). For example, CP-II El Niños produce strong delayed impacts on the boreal summer WPSH, while CP-I El Niños exert weak or nonexistent impacts on the WPSH.

ENSO diversity studies (Capotondi et al., 2015; Yu et al., 2017) suggest that the generation of EP El Niño is closely associated with thermocline variations along the equatorial Pacific, while this is not necessarily the case for CP El Niños. Other generation mechanisms have been suggested for CP El Niños, including horizontal ocean advection in the tropical Pacific (Kug et al., 2009), subtropical North Pacific forcing (Wang, Chen, et al., 2019; Yu & Kim, 2011; Yu et al., 2010), South Pacific forcing (Ding et al., 2017; Guan et al., 2014; Hong et al., 2014), forcing from the Indian Ocean (Yu et al., 2009) and forcing from the Atlantic Ocean (Ham et al., 2013; Jiang & Li, 2021; Park et al., 2019; L. Wang et al., 2017; Yu et al., 2015). Particular attention has been paid to examining the relationship between CP El Niño and the Pacific Meridional Mode (PMM) (Chiang & Vimont, 2004) or the seasonal footprinting mechanism (SFM) (Fang & Yu, 2020; Vimont et al., 2001) in the subtropical Pacific. It has been suggested that SST anomalies induced by extratropical atmospheric disturbances in the northeastern Pacific can be sustained by the wind-evaporation-SST (WES) feedback (Xie & Philander, 1994) for several seasons; and at the same time spread from the northeastern Pacific to the tropical central Pacific to trigger a CP El Niño event. This subtropical Pacific ocean-atmosphere coupling process is referred to as the SFM, while the associated subtropical Pacific SST and surface wind anomaly patterns are referred to as the PMM.

However, as mentioned, only CP-II El Niño is accompanied by positive SST anomalies in the northeastern subtropical Pacific (X. Wang, Guan, et al., 2019). This subtropical-connection feature is absent in CP-I El Niño. This difference prompts us to consider the possibility that these two subtypes of CP El Niño are associated with different generation mechanisms, despite the fact that both are similar in having large SST anomalies in the central tropical Pacific. The objective of this paper is to identify the generation mechanisms of the CP-I and CP-II El Niños. A better understanding of the generation mechanisms can help understand how these two subtypes of CP El Niño may change in the future.

## 2. Data and Methods

In this study, monthly SST data is from Hadley Center Sea Ice and SST data set with a 1.0° × 1.0° horizontal resolution (Rayner et al., 2003). Monthly surface wind and latent heat flux data are from the National Centers for Environmental Prediction/National Center for Atmospheric Research Reanalysis (Kalnay et al., 1996) at a horizontal resolution of 2.5° × 2.5°. Monthly SSH data are from the German contribution of the Estimating the Circulation and Climate of the Ocean project (Köhl, 2015) with a resolution of 1.0° × 1.0°. The historical and RCP8.5 simulations produced by CanESM2, FGOALS-s2, GFDL-ESM2M, GISS-E2-R-CC, and MIROC5 are used in this study. The historical simulation covers the period 1950–2004, while the RCP85 simulation covers the period 2045–2099. Except for the model simulations, all analyses are performed for the period 1950–2016. Anomalies are defined as the deviations from the monthly climatological cycle calculated from the analysis period with the linear trends removed.

During the analysis period, there are seven EP El Niño events (1951/1952, 1965/1966, 1972/1973, 1976/1977, 1982/1983, 1997/1998, 2015/2016), four CP-I El Niño events (1963/1964, 1987/1988, 1990/1991, 2002/2003), and six CP-II El Niño events (1968/1969, 1979/1980, 1991/1992, 1992/1993, 2004/2005, 2009/2010). The following procedure was used to identify El Niño types in the data and CMIP5 simulations. We first use the Niño3 SST index to identify EP Niño events and the El Niño Modoki (EMI) index of Ashok et al. (2007) to identify CP Niño events. We then use the El Niño Modoki-II (MII) index of X. Wang, Tan, and Wang (2018) to further separate CP Niño events into the CP-I and CP-II types. If a CP El Niño event has an MII index larger than 1.5 standard deviations, that event is classified as a CP-II type. Otherwise, it is classified as a CP-I type. Here, the EMI is defined as the difference between SST anomalies averaged over the central Pacific (10°S–10°N, 165°E−140°W) and the anomalies averaged over the western (10°S–20°N, 125°–145°E) and eastern (15°S–5°N, 110°–70°W) Pacific. Following X. Wang, Tan, and Wang (2018), the MII index is defined as the leading mode of a temporal EOF analysis applied to the following three time series: the Niño4 index, the EMI index, and an index of the relative vorticity averaged over the northwestern Pacific near the Philippines during autumn. Since CP-II El Niño events are characterized by large SST anomalies in the Niño4 region, a tri-polar SST anomaly represented by the EMI, and an anomalous cyclone over the Northwestern Pacific during developing autumn (X. Wang, Tan, & Wang, 2018), the MII index can be considered as a way to quantify the intensity of the CP-II component of a CP El Niño event (Figure S1). A CP El Niño with a large value of the MII index is classified to be a CP-II event, otherwise, it is classified as a CP-I event. In our

analyses, Years (−1), (0), and (1) refer, respectively, to the preceding, developing, and decaying years of an El Niño event.

Indices of the PMM and AM are also used in this study. The monthly PMM index is defined as monthly SST anomalies averaged over the northeastern Pacific (21°–25°N and 138°–142°W) following Zhang et al. (2014). The AM index is defined as the 850 hPa zonal wind anomalies averaged over 5°S −15°S and 110°–130°E following Kajikawa et al. (2010). Stronger-than-normal PMM events and weaker-than-normal Australian winter monsoon events are respectively defined as those events during which the DJF values of the PMM index and the JJA values of the AM index are larger than 0.7 standard deviations.

A pair of forced ocean experiments is performed with the Parallel Ocean Program (POP) ocean model module of the Community Earth System Model version 1.2.2 (Hurrell et al., 2013). The model has a 1° horizontal resolution with enhanced meridional resolution (1/3°) in the tropics and 60 vertical levels. In the control run, the POP is spun up for 30 years with monthly climatological winds. The June conditions from the last 20 years of this control run were then used as the initial conditions to launch a 20-member ensemble set of weak monsoon runs. The monsoon run is integrated for 12 months, during which the model is forced with wind anomalies associated with a weak AM during June, July, and August and monthly climatological winds during the rest of the calendar year. The weak monsoon winds are imposed only in a region between 20°S–20°N and 90°–150°E and are composed of the sum of the climatological winds and 5 times the wind anomalies regressed onto the AM index. Ensemble means are then calculated from the monsoon run to calculate differences with the 20-years mean of the control run for analyses presented in the main text.

## 3. Results

### 3.1. Distinct SST Evolution Patterns in the Indo-Pacific Oceans

We first examine the evolutions of SST anomalies in the equatorial Indo-Pacific Oceans (5°S–5°N) composited for the three types of El Niño events. During the EP El Niño (Figure S2), positive SST anomalies appear first along the eastern equatorial Pacific in boreal spring (March(0)–April(0)–May(0)), expand westward during the following seasons, and peak during boreal winter (December(0)–January(+1)–February(+1); D(0)JF(+1)). During both subtypes of the CP El Niño (Figures 1a and 1b), positive SST anomalies are located mostly in the central tropical Pacific. However, these two subtypes are significantly different in three aspects of their SST evolutions. First, their SST anomalies during and immediately before the onset stages (i.e., from fall of Year [−1] to spring of Year [0]) are different. While both types have their positive SST anomalies appear first near 180°E during preceding autumn (September[−1]–October[−1]–November[−1]; SON[−1]), the anomalies during SON(−1) develop in the same longitudinal region for the CP-II El Niño (Figure 1b) but propagate from the far western Pacific (around 120°E) for the CP-I El Niño (Figure 1a). This distinction is clearly revealed in Figure S3, which shows the composite evolution of equatorial (5°S–5°N) SST anomaly differences between the CP-I El Niño and CP-II El Niño. Significant and positive SST anomaly differences appear in the far western Pacific (near 120°E) from summer to autumn of Year (−1).

The second difference appears in their transition patterns. The CP-I El Niño is preceded and followed by a cold phase (Figure 1a). This cyclic transition pattern is similar to, although weaker than, that observed for the EP El Niño (Figure S2). Such a cyclic transition pattern does not frequently occur for the CP-II El Niño (Figure 1b). This subtype is preceded and followed by near-neutral conditions in the tropical Pacific. Such a transition pattern is considered an episodic transition pattern (Yu & Fang, 2018). The charged-discharged mechanism (Jin, 1997) of El Niño-Southern Oscillation (i.e., related to thermocline variations along the equatorial Pacific) tends to produce mostly the cyclic transition pattern, while the PMM produces the episodic transition pattern (Yu & Fang, 2018). This is evidence that the generation of the CP-II El Niño may be related to the PMM in the subtropical Pacific.

The third difference between these two subtypes of CP El Niño is their associated SST anomalies in the Indian Ocean (Figure S3). And this SST anomaly difference between CP-I and CP-II El Niño is significantly positive in the equatorial Indian Ocean. It is known that significant positive SST anomalies appear in the Indian Ocean 3–6 months after the EP El Niño (Figure S2) through an atmospheric bridge mechanism (Klein et al., 1999). In contrast, the CP-II El Niño is accompanied by weak Indian Ocean warming (Figure 1b). Interestingly, significant Indian Ocean warming does occur during the CP-I El Niño (Figure 1a).
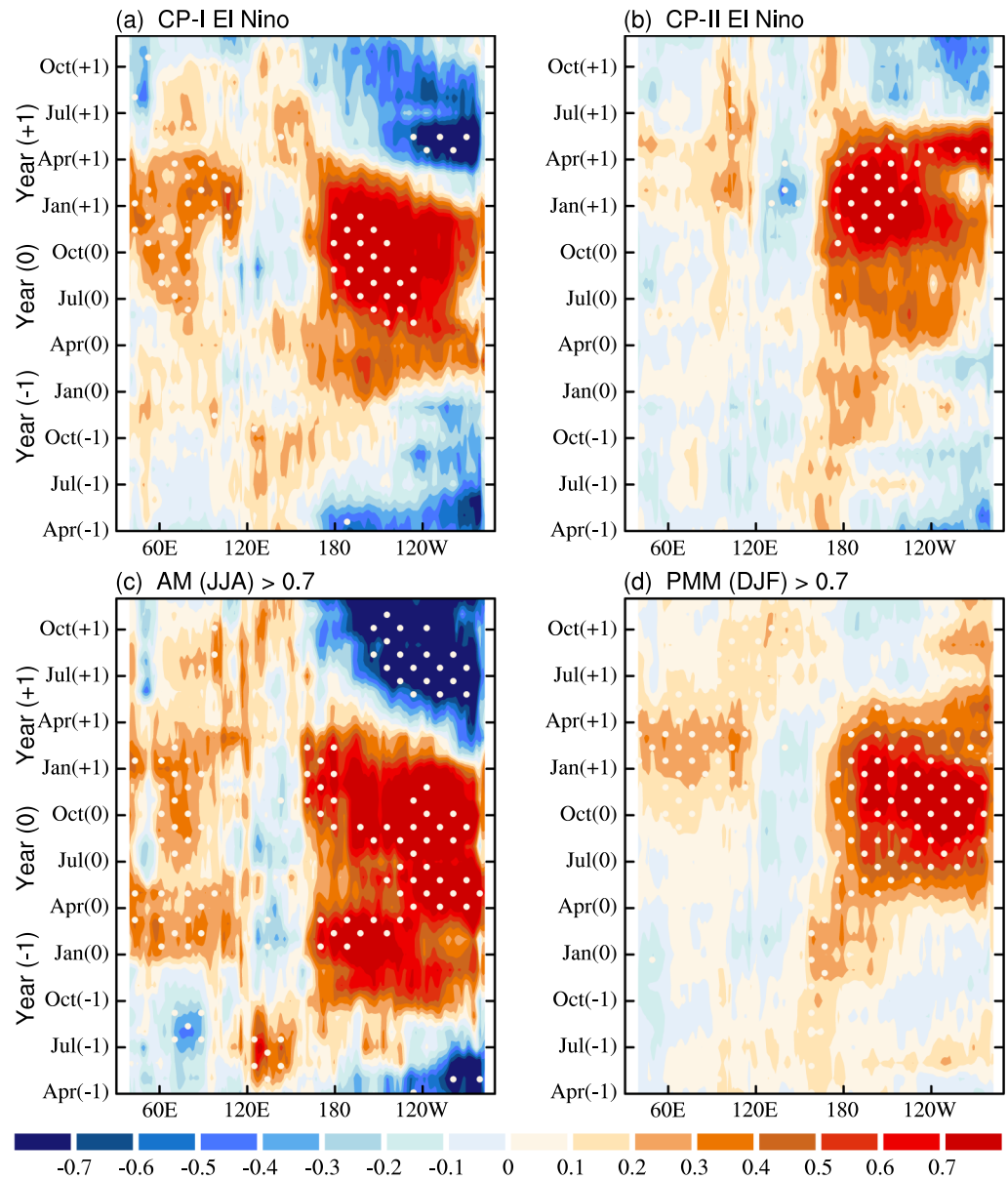
**Figure 1.** Composite evolutions of equatorial (5°S–5°N) sea surface temperature anomalies (°C). Composites for the Central Pacific (CP)-I El Niño (a), CP-II El Niño (b), weaker-than-normal Australian winter monsoon (c), and strong positive Pacific Meridional Mode (PMM) index (d). Year (−1), (0), and (+1) in Y-axis correspond to the preceding, developing, and decaying years of El Niño. The composite year of the weaker-than-normal Australian winter monsoon is labeled as Year (−1) in Figure 1c (i.e., centered at July [−1]). The composite year of strong positive PMM is labeled as Year (−1) in Figure 1d (i.e., centered at Jan [0]). The white-dotted areas denote regions where the composites exceed the 90% significance level based on a Student's t test.

### 3.2. Different Generation Mechanisms for the CP-I and CP-II El Niños

The above SST anomaly patterns suggest that the CP-II El Niño is likely to be generated by the PMM in the subtropical Pacific, while the CP-I El Niño by processes in the far western Pacific yet to be identified. Figure 1a indicates that positive SST anomalies first appear around 120°E during the boreal summer of Year (−1) and later expand eastward toward the central tropical Pacific to onset the CP-I El Niño. This is the region where and the season when the Australian winter monsoon takes place. A model experiment study (Yu et al., 2009) found that Asian-Australian monsoon variability can excite surface wind anomalies in the

western Pacific that force SST variability in the tropical central Pacific. It is possible that the AM is responsible for the generation of the CP-I El Niño.

To examine the possible linkages between the CP-I El Niño and AM and between the CP-II El Niño and PMM, we show the evolutions of equatorial SST anomalies composited from strongly below-normal Australian winter monsoon events (Figure 1c) and strong positive PMM events (Figure 1d). Since it is the AM during the June–July–August (JJA) season that is, hypothesized to trigger El Niño, the composite year of the below-normal Australian winter monsoon is labeled as Year (−1) in Figure 1c. This figure confirms that significant positive SST anomalies appear around 120°E during JJA(−1) when the Australian winter monsoon is weaker than normal. These anomalies then propagate eastward into the Pacific Ocean during the following season. The eastward-propagating anomalies arrive at the central tropical Pacific (around 180°E) during SON(−1) and develop into an El Niño event that resembles the CP-I El Niño. The similar SST anomaly evolution in Figures 1a and 1c is strong evidence that the CP-I El Niño is produced by variations in the Australian winter monsoon. Also, to make sure that our composite results are not sensitive to the criterion used (i.e., 0.7 standard deviations) to select weaker-than-normal Australian winter monsoon events and stronger-than-normal PMM events, we repeat the composite analyses presented in Figures 1c and 1d with different criteria. We obtain similar results when we using 0.6, 0.8, and 1 standard deviations as the case selection criterion in the composite analysis (Figure S4).

Since it is the boreal winter PMM that is, it triggers the CP-II El Niño during the following year, so the composite year of the strong positive PMM is labeled as Year (−1) in Figure 1d. This figure shows that positive SST anomalies appear in the central tropical Pacific during D(−1)JF(0), and then gradually develop into a CP El Niño event that peaks during D(0)JF(+1). The evolution of the PMM composited SST anomalies is similar to that composited for the CP-II El Niño (cf., Figures 1b and 1d). This result confirms that the CP-II El Niño is triggered by the PMM originating from the subtropical Pacific.

While previous studies have detailed how the PMM triggers the onset of the CP El Niño (specifically the CP-II) through the WES mechanism (Yeh, Wang, et al., 2015; Yu & Kim, 2011; Yu et al., 2017), it is not known how the Australian winter monsoon triggers the onset of the CP-I El Niño. The climatological Australian winter monsoon is characterized by surface easterly winds over Northern Australia and Maritime Continent (Figure S5). A weaker-than-normal winter monsoon produces westerly anomalies over these regions, which then reduce surface latent heat fluxes leading to warm SST anomalies (Figures 2a and 2d). This explains the anomalous surface warming around 120°E observed in the Australian winter monsoon composite (Figure 1c) and the CP-I El Niño composite during JJA(−1) (Figure 1a). The oceans north of Australia and near the Maritime Continent are also the regions where the Indonesian Throughflow (ITF) transports warm water from the equatorial Pacific to the Indian Ocean (Gordon, 2005; Gordon & Susanto, 1999; Yuan et al., 2011). This hypothesis is examined and shown in Figure S6a, where we display the lead-lag correlations between ITF and AM indexes during JJA. The figure indicates that positive AM index values in JJA can significantly reduce the ITF transports 1 month later. This is because the monsoon-associated westerly anomalies can decrease the transport of warm water into the eastern Indian Ocean through the three major outflow channels of the ITF (Lombok Strait, the Ombai Strait, and the Timor Strait along the Sumatra–Java island chain) (Potemra & Schneider, 2007; Wyrtki, 1987). The ITF is mostly composed of North Pacific water from the Mindanao Current (Gordon, 2005). Thus, the reduced transport allows warm water to accumulate in the far western tropical North Pacific, resulting in positive SST and sea surface height (SSH) anomalies in the region (Figure 2g). The accumulated warm water in the far western equatorial Pacific can excite downwelling Kelvin waves that propagate rapidly eastward, which is reflected in the evolution of SSH anomalies (Figures 2g–2i and 3). The Kelvin waves spread positive SSH anomalies into the central tropical Pacific (around 180°E) during autumn of Year (−1) to later trigger a CP-I El Niño event (Figures 3, 1a, and 1c).

Since the surface latent heat fluxes in the NCEP/NCAR reanalysis used in Figures 2d–2f are model generated without any constraint from observations (Kumar & Hu, 2012), we repeated the analysis with the objectively analyzed air-sea flux dataset (Yu & Weller, 2007) and obtained broadly similar results (Figure S7). Also, we notice that the AM-induced SSH anomalies can propagate eastward and reach into the eastern tropical Pacific (see Figure 3), which may cause thermocline variations and potentially give rise to EP El Niño events. The weak relationship between the AM and the EP El Niño is supported by the fact that the evolution of the SSH anomalies associated with the EP El Niño is different from the evolution of the
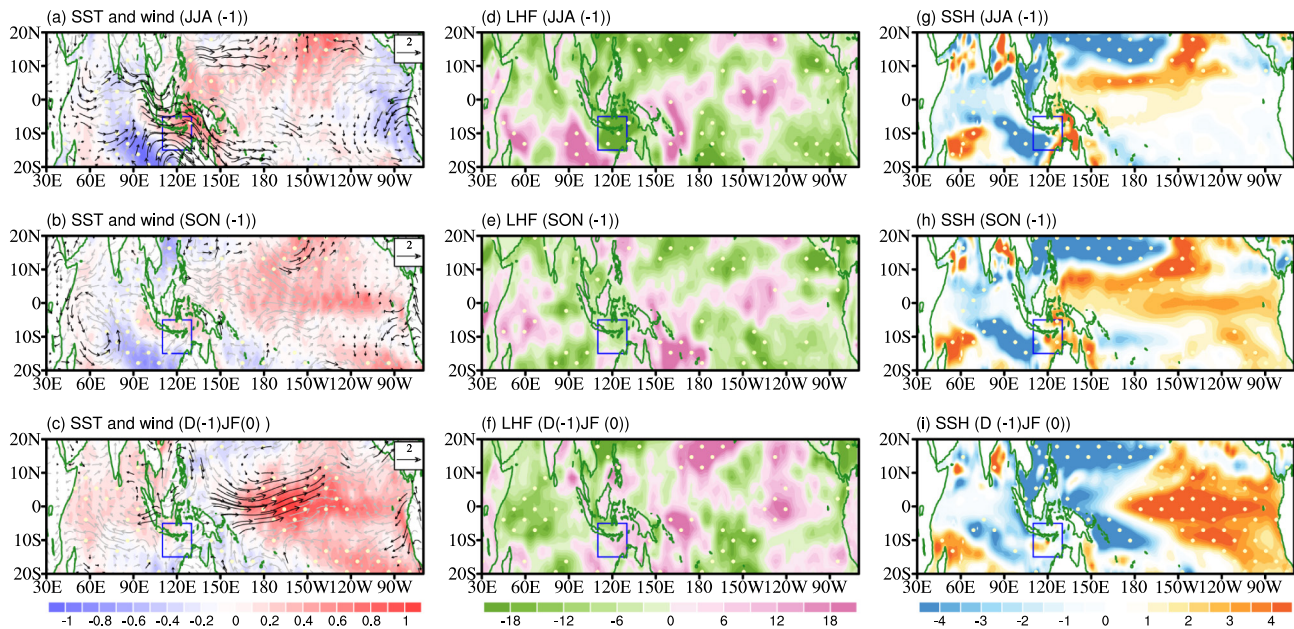
**Figure 2.** Composite evolutions in the Tropical Indo-Pacific Oceans. Composite evolutions of 850 hPa wind (vectors in a–c), sea surface temperature (SST) (shading in a–c), surface latent heat flux (d–f), and sea surface height (SSH) (g–i) anomalies for the weaker-than-normal Australian winter monsoon year from austral winter (June–July–August; JJA) to the following September–October–November (SON) and December–January–February (DJF) seasons. Year (−1) refers to the composite year and is used here for the sake of comparing the evolutions with the anomalies observed in the year preceding the onset of the Central Pacific El Niño composite. Years of weak Australian winter monsoon (AM) are identified as those with an AM index in JJA that is, greater than 0.7 standard deviations. Blue boxes denote the region used to define the AM index. The white-dotted areas and bold vectors mark the composites that exceed the 90% significance level based on a Student's t test. Units are ms$^{-1}$ for wind, °C for SST, Wm$^{-2}$ for surface heat flux, and cm for SSH.
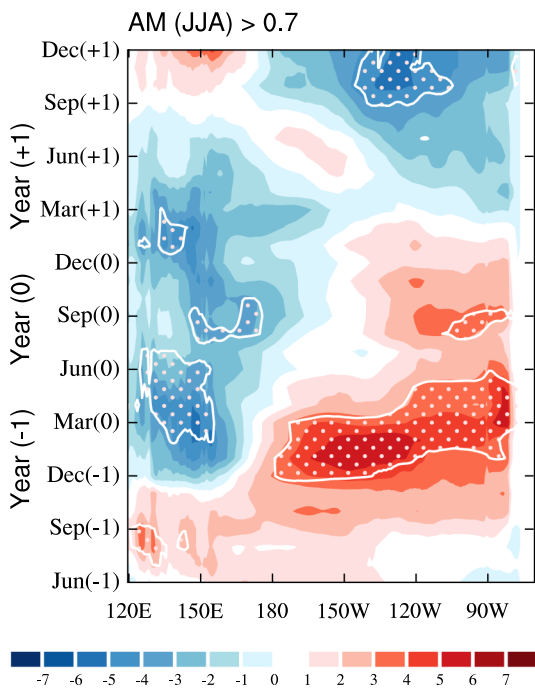


**Figure 3.** Composite evolutions of equatorial (5°S–5°N) sea surface height (SSH) anomalies (cm). As in Figure 1 but for the equatorial SSH (shading) anomalies in Pacific composited for the weaker-than-normal Australian winter monsoon.

AM-induced SSH anomalies (cf., Figures 3 and S8). The main component of the SSH anomalies during the EP El Niño originates in the western Pacific during the autumn of Year (−1) (Figure S8). At this time, the AM-induced SSH anomalies have already propagated into the central Pacific (Figure 3). Also, the AM-induced SSH anomalies arrive in the tropical eastern Pacific during early spring of Year (0) (Figure 3), while the SSH anomalies associated with the EP El Niño arrive in the eastern Pacific during the late spring and early summer (Figure S8).

To further examine whether AM-associated wind anomalies can trigger the CP-I El Niño through the above processes, we perform a pair of forced experiments with an ocean general circulation model. The experiments include a control run where the ocean model is forced by monthly climatological winds and a monsoon run where the model is forced by the anomalous winds associated with a weaker-than-normal AM during austral winter (i.e., during JJA[−1]). The monsoon run is a 20-member ensemble. The differences between the monsoon run and the control run confirm that (a) the ITF transport in JJA is reduced by 16% from the control run to the weak monsoon run (Figure S6b), (b) the weak Austrian monsoonal forcing induces positive SSH anomalies in the tropical western Pacific (Figure 4d), (c) the SSH anomalies propagate eastward into the equatorial central Pacific (Figure 4e) as downwelling Kelvin waves (Figure S9), and (d) anomalous warming then appears in the equatorial central Pacific during SON(−1) (Figure 4b) and continue to spread eastward afterward (Figure 4c).

A case study was performed, and it was found that three of the four observed CP-I El Niños occur after a weak Australian winter monsoon
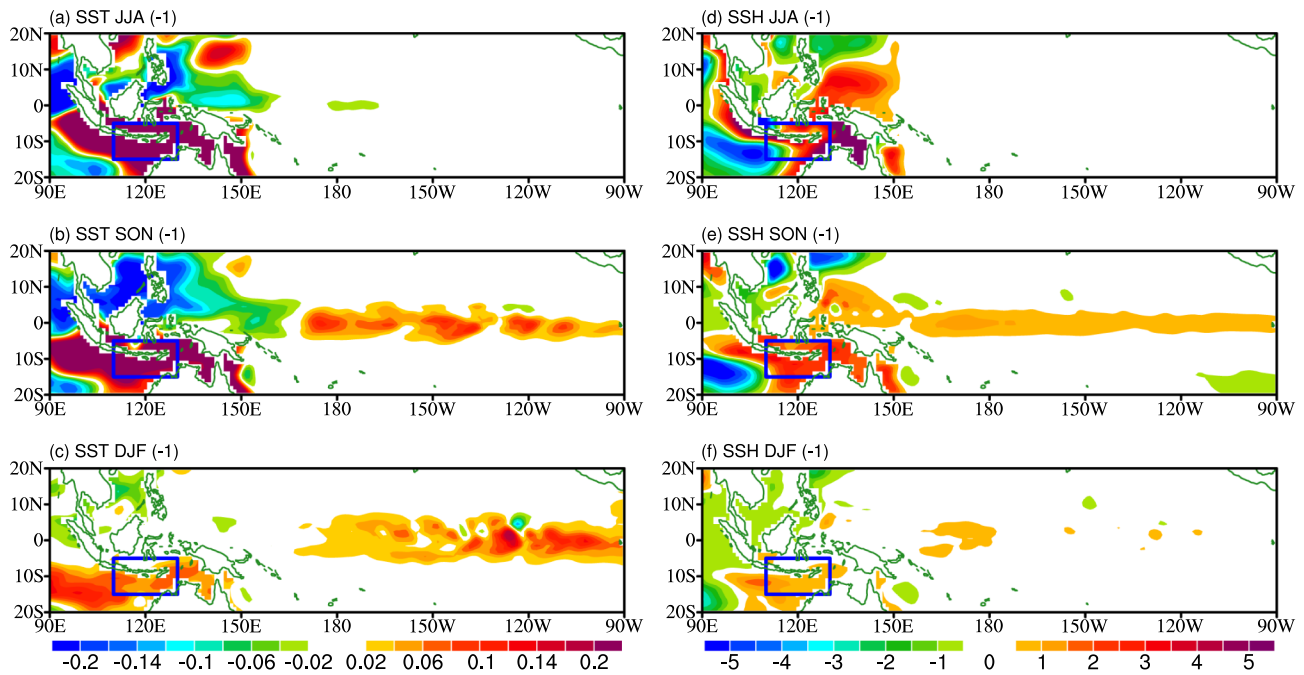
**Figure 4.** Seasonal averaged (a–c) sea surface temperature (°C) and (d–f) sea surface height differences (cm) between the ensemble mean of the 20-member monsoon run and the control run of the forced OGCM experiment. The seasons shown are June–July–August (JJA) (a and d), September–October–November (SON) (b and e), and December–January–February (DJF) (c and f). The blue box denotes the region where the Australian winter monsoon index is defined and where the anomalous monsoonal winds are prescribed in the monsoon run.

(Table S1). The Australian winter monsoon index has positive values (i.e., weaker-than-normal monsoon) during the entire austral winter season of the 1987–1988 and 1990–1991 events and during the late summer months of the 2002–2003 event. A weak winter monsoon was absent only for the 1963–1964 event. This result is consistent with the evolution of equatorial SST anomalies during these four CP-I El Niño events (1963/1964, 1987/1988, 1990/1991, and 2002/2003) (Figure S10). Except for the 1963/1964 event, CP-I El Niños all show positive SST anomalies in the far western equatorial Pacific (around 120°E) during the JJA(−1) season. The possible linkage between the Australian winter monsoon and the generation of the CP-I El Niño is supported by most of the CP-I El Niño events during the analysis period.

We notice from Figure 1a that the warm anomalies in the far western Pacific during JJA(−1) of the CP-I El Niño are also accompanied by cold SST anomalies in the tropical eastern Pacific. To exclude the possibility that the far western Pacific warming is related to this La Niña condition rather than the weak Australian monsoon, we composite the equatorial SST anomalies from all 20 La Niña events during the analysis period. The composite shows that La Niña does not produce significant warming in the far western Pacific during JJA after La Niña (Figure S11). Also, to determine whether the weaker-than-normal Australian winter monsoon is induced by a La Niña event during its decaying JJA, we examine the AM index values during the decaying JJA seasons of the 20 La Niña events observed during 1950–2016. As shown in Figure S12, some (12 of 20) La Niña events are associated with weaker-than-normal Australian winter monsoons but others (8 of 20) are associated with stronger-than-normal Australian winter monsoons. The composite Australian winter monsoon (i.e., the gray bar in Figure S12) is not significantly weaker than normal. Thus, there is no clear evidence that the weaker-than-normal Australian winter monsoon is induced by a preceding La Niña event.

We also notice in Figure 2a that a PMM-like structure appears in the SST evolution composited for weaker-than-normal winter AMs. We conduct a lead-lagged correlation analysis of the monthly PMM index with the austral winter (JJA) AM index to clarify the relationship between the Australian winter monsoon and the PMM. The result (Figure S13) indicates that a weaker-than-normal Australian winter monsoon may induce a positive PMM structure during the following months. It is possible that the AM-induced anomalous warming around Australia may excite a Rossby wave train that propagates into the extra-tropical Pacific (Fang & Yu, 2020), which can then impact subtropical Pacific trade winds. This tropical-extratropical
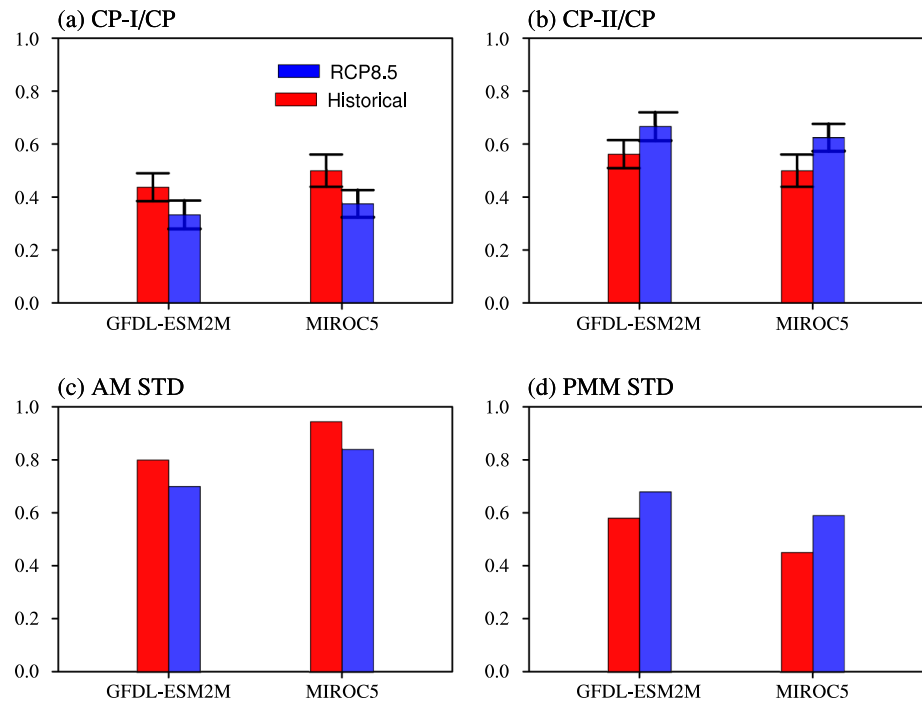
**Figure 5.** Future changes in the ratios of the Central Pacific (CP)-I and CP-II El Niños and the standard deviations of the Australian winter monsoon (AM) and Pacific Meridional Mode (PMM) indices. The ratios of the CP-I (a) and CP-II (b) El Niños to total CP El Niño events in the historical (red) and RCP8.5 (blue) simulations of GFDL-ESM2M and MIROC5 (a and b). The standard deviation of AM (c) and PMM (d) indices in the historical (red) and RCP8.5 (blue) simulations of GFDL-ESM2M and MIROC5 (c and d). The black bars in (a and b) denote the 90% confidence intervals.

interaction may be a reason why a PMM-like SSTA pattern appears in the AM composite. We have further conducted a conditional composite with large AM index events that were accompanied by small values of the PMM index in JJA to confirm that it is the weaker-than-normal winter AM that induces the CP-I El Niño (Figure S14).

### 3.3. Future Changes in the CP-I and CP-II El Niños

There are pronounced inter-decadal variations of the intensity and frequency of ENSO in the observations, such as an increasing frequency of CP El Niños since the 1990s (e.g., Hu et al., 2020; Yu et al., 2012). But there is no consensus on the change of CP El Niño as the global atmosphere warms. Some studies suggest that the CP El Niño will occur frequently (Yeh, Kug, et al., 2009) and intensify (S. T. Kim & Yu, 2012) in the future, while other studies suggest no significant changes (L'Heureux, et al., 2013; Xu et al., 2017). Stevenson et al. (2021) indicated that model biases may lead to uncertainties in the projections of extreme El Niños. With these limitations in mind, we make an effort to project future changes in CP-I and CP-II El Niño as global climate changes. This projection is of interest because the two subtypes of CP El Niño produce different and important climate impacts. A previous study (X. Wang, Chen, et al., 2019) has identified five models in Coupled Model Inter-comparison Project Phase 5 (CMIP5) (CanESM2, FGOALS-s2, GFDL-ESM2M, GISS-E2-R-CC, and MIROC5) to be capable of simulating CP El Niño. We find that only the GFDL-ESM2M and MIROC5 reproduce the observed linkages between the two subtypes and the AM (Figure S15) and the PMM (Figure S16). In these two models, both CP-I El Niño events and weak Australian winter monsoons are associated with an eastward spreading of warm SST anomalies from around 120°E to 180°E during August(-1)-December(-1). Their simulated CP-II El Niño and the PMM share similar in-situ developments of warm SST anomalies around 180°E.

These two models are considered to be the best and their future projections are compared with the projections from the other three models. Figure 5 shows the ratios (by numbers) of CP-I and CP-II El Niños to total CP El Niño events in their historical and high emissions scenario (RCP8.5) simulations. The two best

models consistently project the frequency of occurrence of CP-I El Niño events to decrease in the future (Figure 5a) while the frequency of CP-II El Niño events is projected to increase (Figure 5b). The changes are statistically significant at the 90% significance interval in the MIROC5 projection but slightly below this level of significance in the GFDL-ESM2M projection. Yu et al. (2012) suggested that the frequency of occurrence of the CP El Niño events is projected to increase in the future. The present results allow for a refinement of this conclusion to state that the increased occurrence is for CP-II El Niño events only. Based on the generation mechanisms of these two subtypes of the CP El Niño, we expect the PMM activity to increase and the AM variability to decrease in the future. This is confirmed by these two best models. The standard deviation of their AM index decreases (Figure 5c) but that of their PMM index increases in the RCP8.5 simulation (Figure 5d) compared to the historical simulation. This result adds additional support to our suggestion that the generation of the CP-I El Niño is linked to the AM and the generation of the CP-II El Niño to the PMM.

## 4. Summary and Discussion

In this study, we conducted statistical analyses with reanalysis products, case studies, CMIP5 model simulations, and model experiments to show that the CP-I and CP-II El Niños are indeed different and should be treated as two different types. They possess different SST evolution patterns in the Indo-Pacific Oceans, distinct generation mechanisms, and can respond differently to global warming. The CP-I El Niño is triggered by a weaker-than-normal Australian winter monsoon in the preceding year, while the onset of CP-II El Niño is related to the PMM. Our cases studies indicate that three of four CP-I El Niño events were preceded by a positive AM index (i.e., weaker-than-normal AM) in the previous boreal summer. This result further supports our conclusion that the CP-I El Niño is primarily related to the AM. Other factors might be involved in the onset of the CP-I El Niño that was not preceded by a positive AM index. Duan et al. (2020) indicated that the Indian Ocean Dipole (IOD) mode can induce the variation of SSH anomalies in the western Pacific. Whether the IOD mode can impact the onset of the CP-I El Niño deserves further research.

Our results have many implications. In the future, the CP El Niño will become more related to the PMM and onset more frequently from the west coast of North America. Subtropical Pacific information will be more important in the prediction of CP El Niño events. Also, SST variability in the Indian Ocean is likely to be less influenced by El Niño and become more dominated by its own internal dynamics. It should be noted that some of the results presented in this study are based on relatively small sample sizes in the observations, which is a common challenge faced by most ENSO diversity studies and can only be addressed when longer observational datasets become available.

## Data Availability Statement

The SST data of Hadley Center Sea Ice and Sea Surface Temperature data set were downloaded from their site (http://www.metoffice.gov.uk/hadobs/hadisst/data/download.html). Monthly surface wind and latent heat flux data from the National Centers for Environmental Prediction/National Center for Atmospheric Research Reanalysis at a horizontal resolution of 2.5° × 2.5° were downloaded from NOAA (https://psl.noaa.gov/data/gridded/data.ncep.reanalysis.derived.pressure.html and https://psl.noaa.gov/data/gridded/data.ncep.reanalysis.derived.surfaceflux.html). Monthly SSH data sets from the German contribution to the Estimating the Circulation and Climate of the Ocean project were downloaded from the Integrated Climate Data Center (https://icdc.cen.uni-hamburg.de/thredds/catalog/ftpthredds/EASYInit/GECCO2/regular_1x1_grid/catalog.html?dataset=ftpthreddsscan/EASYInit/GECCO2/regular_1x1_grid/zeta29_34_70.nc) with a resolution of 1.0° × 1.0°.

## References

Ashok, K., Behera, S. K., Rao, S. A., Weng, H., & Yamagata, T. (2007). El Niño Modoki and its teleconnection. *Journal of Geophysical Research*, *112*, C11007. https://doi.org/10.1029/2006jc003798

Capotondi, A., Wittenberg, A. T., Newman, M., Di Lorenzo, E., Yu, J. Y., Braconnot, P., et al. (2015). Understanding ENSO diversity. *Bulletin of the American Meteorological Society*, *96*(6), 921–938. https://doi.org/10.1175/BAMS-D-13-00117.1

Chen, M., Chang, T.-H., Lee, C.-T., Fang, S.-W., & Yu, J.-Y. (2021). A study of climate model responses of the western Pacific subtropical high to El Niño diversity. *Climate Dynamics*, *56*, 581–595. https://doi.org/10.1007/s00382-020-05500-2

Chen, M., Yu, J.-Y., Wang, X., & Jiang, W. (2019). The changing impact mechanisms of a diverse El Niño on the western Pacific subtropical high. *Geophysical Research Letters*, *46*(2), 953–962. https://doi.org/10.1029/2018GL081131

Chiang, J. C. H., & Vimont, D. J. (2004). Analogous meridional modes of atmosphere-ocean variability in the tropical Atlantic and tropical Pacific. *Journal of Climate*, *17*, 4143–4158. https://doi.org/10.1175/jcli4953.1

Ding, R., Li, J., Tseng, Y.-H., Sun, C., & Xie, F. (2017). Joint impact of North and South Pacific extratropical atmospheric variability on the onset of ENSO events. *Journal of Geophysical Research*, *122*, 279–298. https://doi.org/10.1002/2016jd025502

Duan, J., Li, Y., Zhang, L., & Wang, F. (2020). Impacts of the Indian Ocean Dipole on sea level and gyre circulation of the western tropical Pacific Ocean. *Journal of Climate*, *33*, 4207–4228. https://doi.org/10.1175/jcli-d-19-0782.1

Fang, S.-W., & Yu, J.-Y. (2020). A control of ENSO transition complexity by tropical Pacific mean SSTs through Tropical-Subtropical interaction. *Geophysical Research Letters*, *47*, e2020GL087933. https://doi.org/10.1029/2020GL087933

Gordon, A. L. (2005). Oceanography of the Indonesian seas and their throughflow. *Oceanography*, *18*, 14–27. https://doi.org/10.5670/oceanog.2005.01

Gordon, A. L., & Susanto, R. D. (1999). Makassar strait transport: Initial estimate based on Arlindo results. *Marine Technology Society Journal*, *32*, 34–45.

Guan, Y., Zhu, J., Huang, B., Hu, Z.-Z., & Kinter, J. L. (2014). South Pacific Ocean dipole: A predictable mode on multiseasonal time scales. *Journal of Climate*, *27*, 1648–1658. https://doi.org/10.1175/jcli-d-13-00293.1

Ham, Y.-G., Kug, J.-S., Park, J.-Y., & Jin, F.-F. (2013). Sea surface temperature in the north tropical Atlantic as a trigger for El Niño/Southern Oscillation events. *Nature Geoscience*, *6*, 112–116. https://doi.org/10.1038/ngeo1686

Hong, L.-C., Ho, L., & Jin, F.-F. (2014). A Southern Hemisphere booster of super El Niño. *Geophysical Research Letters*, *41*, 2142–2149. https://doi.org/10.1002/2014gl059370

Hu, Z.-Z., Kumar, A., Huang, B., Zhu, J., L'Heureux, M., McPhaden, M., & Yu, J.-Y. (2020). The interdecadal shift of ENSO properties in 1999/2000: A review. *Journal of Climate*, *33*(11), 4441–4462. https://doi.org/10.1175/jcli-d-19-0316.1

Hurrell, J. W., Holland, M. M., Gent, P., Ghan, S., Kay, J. E., Kushner, P., et al. (2013). The community earth system model: A framework for collaborative research. *Bulletin of the American Meteorological*, *94*, 1339–1360. https://doi.org/10.1175/bams-d-12-00121.1

Jiang, L., & Li, T. (2021). Impacts of tropical North Atlantic and Equatorial Atlantic SST anomalies on ENSO. *Journal of Climate*, 5635–5655. https://doi.org/10.1175/jcli-d-20-0835.1

Jin, F.-F. (1997). An equatorial recharge paradigm for ENSO. Part I: Conceptual model. *Journal of the Atmospheric Sciences*, *54*, 811–829. https://doi.org/10.1175/1520-0469(1997)054<0811:aeorpf>2.0.co;2

Kajikawa, Y., Wang, B., & Yang, J. (2010). A multi-time scale Australian monsoon index. *International Journal of Climatology*, *30*, 1114–1120. https://doi.org/10.1002/joc.1955

Kalnay, E., Kanamitsu, M., Kistler, R., Collins, W., Deaven, D., Gandin, L., et al. (1996). The NCEP/NCAR 40-year reanalysis project. *Bulletin of the American Meteorological Society*, *77*(3), 437–471. https://doi.org/10.1175/1520-0477(1996)077<0437:tnyrp>2.0.co;2

Kim, J.-W., Chang, T.-H., Lee, C.-T., & Yu, J.-Y. (2021). On the varying responses of East Asian winter monsoon to three types of El Nino: Observations and model hindcasts. *Journal of Climate*, *34*, 4089–4101. https://doi.org/10.1175/jcli-d-20-0784.1

Kim, S. T., & Yu, J.-Y. (2012). The two types of ENSO in CMIP5 models. *Geophysical Research Letters*, *39*, L11704. https://doi.org/10.1029/2012GL052006

Klein, S. A., Soden, B. J., & Lau, N.-C. (1999). Remote sea surface temperature variations during ENSO: Evidence for a tropical atmospheric bridge. *Journal of Climate*, *12*, 917–932. https://doi.org/10.1175/1520-0442(1999)012<0917:rsstvd>2.0.co;2

Köhl, A. (2015). Evaluation of the GECCO2 ocean synthesis: Transports of volume, heat and freshwater in the Atlantic. *Quarterly Journal of the Royal Meteorological Society*, *141*, 166–181. https://doi.org/10.1002/qj.2347

Kug, J.-S., Jin, F.-F., & An, S.-I. (2009). Two types of El Niño events: Cold tongue El Niño and warm pool El Niño. *Journal of Climate*, *22*, 1499–1515. https://doi.org/10.1175/2008jcli2624.1

Kumar, A., & Hu, Z.-Z. (2012). Uncertainty in the ocean-atmosphere feedbacks associated with ENSO in the reanalysis products. *Climate Dynamics*, *39*(3–4), 575–588. https://doi.org/10.1007/s00382-011-1104-3

Lee, T., & McPhaden, M. J. (2010). Increasing intensity of El Niño in the central equatorial Pacific. *Geophysical Research Letters*, *37*, L14603. https://doi.org/10.1029/2010gl044007

L'Heureux, M., Collins, D. C., & Hu, Z.-Z. (2013). Linear trends in sea surface temperature of the tropical Pacific Ocean and implications for the El Niño-Southern Oscillation. *Climate Dynamics*, *40*, 1223–1236.

Park, J.-H., Li, T., Yeh, S.-W., & Kim, H. (2019). Effect of recent Atlantic warming in strengthening Atlantic-Pacific teleconnection on interannual timescale via enhanced connection with the Pacific meridional mode. *Climate Dynamics*, *53*(1), 371–387. https://doi.org/10.1007/s00382-018-4591-7

Potemra, J. T., & Schneider, N. (2007). Interannual variations of the Indonesian throughflow. *Journal of Geophysical Research*, *112*, C05035. https://doi.org/10.1029/2006jc003808

Rayner, N. A., Parker, D. E., Horton, E. B., Folland, C. K., Alexander, L. V., Rowell, D. P., et al. (2003). Global analyses of sea surface temperature, sea ice, and night marine air temperature since the late nineteenth century. *Journal of Geophysical Research*, *108*(D14), 4407. https://doi.org/10.1029/2002JD002670

Stevenson, S., Wittenberg, A. T., Fasullo, J., Coats, S., & Otto-Bliesner, B. (2021). Understanding diverse model projections of future extreme El Niño. *Journal of Climate*, *34*(2), 449–464. https://doi.org/10.1175/JCLI-D-19-0969.1

Tan, W., Wang, X., Wang, W., Wang, & C., & Zuo, J. (2016). Different responses of sea surface temperature in the South China Sea to various El Niño events during boreal autumn. *Journal of Climate*, *29*, 1127–1142. https://doi.org/10.1175/JCLI-D-15-0338.1

Tan, W., Wei, Z., Liu, Q., Fu, Q., Chen, M., Li, B., & Li, J. (2020). Different influences of two El Niño types on low-level atmospheric circulation over the subtropical western north Pacific. *Journal of Climate*, *33*, 825–846. https://doi.org/10.1175/jcli-d-19-0223.1

Vimont, D. J., Battisti, D. S., & Hirst, A. C. (2001). Footprinting: A seasonal connection between the tropics and mid-latitudes. *Geophysical Research Letters*, *28*, 3923–3926. https://doi.org/10.1029/2001gl013435

Wang, C., & Wang, X. (2013). Classifying El Niño Modoki I and II by different impacts on rainfall in southern China and typhoon tracks. *Journal of Climate*, *26*(4), 1322–1338. https://doi.org/10.1175/JCLI-D-12-00107.1

Wang, L., Yu, J.-Y., & Paek, H. (2017). Enhanced biennial variability in the Pacific due to Atlantic capacitor effect. *Nature Communications*, *8*, 14887. https://doi.org/10.1038/ncomms14887

Wang, X., Chen, M., Wang, C., Yeh, S. W., & Tan, W. (2019). Evaluation of the relationships between the North Pacific Oscillation and El Niño Modoki in CMIP5 models. *Climate Dynamics*, *52*, 1383–1394. https://doi.org/10.1007/s00382-018-4196-1

Wang, X., Guan, C., Huang, R. X., Tan, W., & Wang, L. (2019). The roles of tropical and subtropical wind stress anomalies in the El Niño Modoki onset. *Climate Dynamics*, *52*, 6586–6597. https://doi.org/10.1007/s00382-018-4534-3

Wang, X., Tan, W., & Wang, C. (2018). A new index for identifying different types of El Niño Modoki events. *Climate Dynamics*, *50*(7), 2753–2765. https://doi.org/10.1007/s00382-017-3769-8

Wang, X., & Wang, C. (2014). Different impacts of various El Niño events on the Indian Ocean Dipole. *Climate Dynamics*, *42*(3–4), 991–1005. https://doi.org/10.1007/s00382-013-1711-2

Wyrtki, K. (1987). Indonesian throughflow and the associated pressure gradient. *Journal of Geophysical Research*, *92*(12), 12941–12946. https://doi.org/10.1029/jc092ic12p12941

Xie, S.-P., & Philander, S. G. H. (1994). A coupled ocean-atmosphere model of relevance to the ITCZ in the eastern Pacific. *Tellus*, *46A*, 340–350. https://doi.org/10.3402/tellusa.v46i4.15484

Xu, K., Tam, C.-Y., Zhu, C., Liu, B., & Wang, W. (2017). CMIP5 projections of two types of El Niño and their related tropical precipitation in the 21st century. *Journal of Climate*, *30*, 849–864. https://doi.org/10.1175/JCLI-D-16-0413.1

Yeh, S.-W., Kug, J.-S., Dewitte, B., Kwon, M.-H., Kirtman, B. P., & Jin, F.-F. (2009). El Niño in a changing climate. *Nature*, *461*, 511–514. https://doi.org/10.1038/nature08316

Yeh, S.-W., Wang, X., Wang, C., & Dewitte, B. (2015). On the relationship between the north Pacific climate variability and the central Pacific El Niño. *Journal of Climate*, *28*, 663–677. https://doi.org/10.1175/jcli-d-14-00137.1

Yu, J.-Y., & Fang, S.-W. (2018). The distinct contributions of the seasonal footprinting and charged-discharged mechanisms to ENSO complexity. *Geophysical Research Letters*, *45*, 6611–6618. https://doi.org/10.1029/2018gl077664

Yu, J. Y., Kao, H. Y., & Lee, T. (2010). Subtropics-related interannual sea surface temperature variability in the Central Equatorial Pacific. *Journal of Climate*, *23*(11), 2869–2884. https://doi.org/10.1175/2010JCLI3171

Yu, J.-Y., Kao, P.-K., Paek, H., Hsu, H.-H., Hung, C.-W., Lu, M.-M., & An, S.-I. (2015). Linking emergence of the Central-Pacific El Nino to the Atlantic Multi-decadal oscillation. *Journal of Climate*, *28*, 651–662. https://doi.org/10.1175/JCLI-D-14-00347.1

Yu, J. Y., & Kim, S. T. (2011). Relationships between extratropical sea level pressure variations and the central Pacific and eastern Pacific types of ENSO. *Journal of Climate*, *24*(3), 708–720. https://doi.org/10.1175/2010JCLI3688.1

Yu, J.-Y., Lu, M.-M., & Kim, S. T. (2012). A change in the relationship between tropical central Pacific SST variability and the extratropical atmosphere around 1990. *Environmental Research Letters*, *7*, 034025. https://doi.org/10.1088/1748-9326/7/3/034025

Yu, J. Y., Sun, F., & Kao, H. Y. (2009). Contributions of Indian Ocean and monsoon biases to the excessive biennial ENSO in CCSM3. *Journal of Climate*, *22*(7), 1850–1858. https://doi.org/10.1175/2008JCLI2706.1

Yu, J. Y., Wang, X., Yang, S., Paek, H., & Chen, M. (2017). Changing El Niño–Southern Oscillation and associated climate extremes. In S.-Y. Wang, J.-H. Yoon, C. Funk, & R. R. Gillies (Eds.), *Book chapter in climate extremes: Patterns and mechanisms. Geophysical Monograph Series* (Vol. 226, pp. 3–38). American Geophysical Union.

Yu, L., & Weller, R. A. (2007). Objectively analyzed air–sea heat fluxes(OAFlux) for the global ocean. *Bulletin of the American Meteorological Society*, *88*, 527–540. https://doi.org/10.1175/bams-88-4-527

Yuan, D., Wang, J., Xu, T., Xu, P., Zhou, H., Zhao, X., et al. (2011). Forcing of the Indian ocean dipole on the interannual variations of the tropical Pacific ocean: Roles of the Indonesian throughflow. *Journal of Climate*, *24*, 3593–3608. https://doi.org/10.1175/2011jcli3649.1

Zhang, H., Clement, A., & Di Nezio, P. (2014). The South Pacific meridional mode: A mechanism for ENSO-like variability. *Journal of Climate*, *27*, 769–783. https://doi.org/10.1175/jcli-d-13-00082.1